Nanoscience and Nanotechnology Letters
Vol. 10, 1–11, 2018

Bio-Inspired Synthesis of Silver Nanoparticles: Anticancer Drug Carrier, Catalytic and Bactericidal Potential

M. Naz[1,7], M. Zahid Qureshi[1], A. Shahbaz[2], A. Haider[3], M. Ikram[4,*], M. Nafees[4], A. Shahzadi[5], T. Bashir[1], S. Ali[4], A. C. Blackburn[6], H. Chen[7], and A. Tricoli[7]

[1] *Biochemistry Lab, Department of Chemistry, Government College University Lahore, 54000, Punjab, Pakistan*
[2] *Clinical Center, Government College University Lahore, 54000, Punjab, Pakistan*
[3] *Department of Clinical Medicine and Surgery, University of Veterinary and Animal Sciences, Lahore, 54000, Punjab, Pakistan*
[4] *Solar Cell Applications Research Lab, Department of Physics, Government College University Lahore, 54000, Punjab, Pakistan*
[5] *University College of Pharmacy, University of the Punjab, Lahore, 54000, Pakistan*
[6] *ACRF Department of Cancer Biology and Therapeutics, The John Curtin School of Medical Research, The Australian National University, Canberra, 2601, Australia*
[7] *Nanotechnology Research Laboratory, Research School of Engineering, The Australian National University, Canberra, 2601, Australia*

Green route was adopted for the synthesis of stable silver nanoparticles (Ag-NPs) using *Cenchrus ciliaris* (*C. ciliaris*) seeds exudates. A variety of techniques were deployed for the characterization of the bio-synthesized Ag-NPs using ultraviolet-visible spectrophotometer-UV_Vis, X-ray diffraction-XRD, scanning electron microscopy-SEM, transmission electron microscopy-TEM and fourier transform infrared spectrometry-FTIR. Increasing *C. ciliaris* concentration leads to a reduction in the particle size accompanied with agglomeration between the NPs. The results demonstrate that Ag-NPs (1-3CC) are less agglomerated and exhibited significant antimicrobial potential against various bacterial strains compared to 4-5CC. In this project performance of nanocatalyst was evaluated on toxic contaminants that exhibit excellent degradation of methylene blue (MB) and congo red (CR) by $NaBH_4$ in an eco-friendly manner. In addition, Ag-NPs were loaded with anticancer drugs (ACD) [doxorubicin (Dox) hydrochloride, and daunorubicin (Dono)] to develop novel drug carrier with high loading capacity and rapid drug adsorption rate to hampered the side effects of ACD. The loading capacity of ACD was investigated as a function of contact time and adsorption dosages had a maximum adsorption capacity of 404.19 and 253.85 mg/g for Dox and Dono respectively. Moreover, kinetic models were conducted to evaluate the adsorption kinetics.

Keywords: *Cenchrus ciliaris*, Ag Nanoparticles, Green Synthesis, Degradation, Drug Loading.

1. INTRODUCTION

Bio-inspired synthesis of nanoparticles is an economical and eco-friendly technique to improve the existing physical and chemical methods.[1] In medical research, Ag-NPs play an important role especially in cancer therapy, radiotherapy, chemotherapy, immunotherapy, thermotherapy imaging, Photodynamic therapy, immunodetection, antimicrobial and anti-angiogenesis.[2,3] Nanotechnology is employed as a tool in sensing,[4] targeted drug delivery,[5] imaging,[6] gene delivery systems,[7] osteogenesis and artificial implants.[8–10]

Synthetic dyes are organic compounds released by variety of industries such as plastic, paper, leather, food, textile, cosmetic, and pharmaceutical industries.[11,12] These effluents from industries result in significant environmental pollution. Azo dye and amines were recognized as potential carcinogens.[13] Reduction of dyes is required before they are let out for land disposal purposes.[13,14]

Cancer is a most prevalent health problem worldwide with millions of death annually.[15] Radiotherapy and chemotherapy are leading treatment options for cancer therapy.[16] The efficiency of chemotherapy, however, is limited by nonspecific cytotoxicity, bioavailability and poor aqueous solubility.[17,18] Targeted drug delivery is strongly

*Author to whom correspondence should be addressed.

recommended in cancer treatment.[19] In general, nanoparticles of 10–200 nm could not be used directly for drug delivery because of their agglomeration and consequently thrombosis.[20, 21] They oxidized readily and induce harmful free radicals.[22] Drug delivery, tissue regeneration and adsorption kinetics, evaluation are the important research areas in recent biomedical science.[23, 24] Metal stabilized polymers have become more popular due to remarkable properties and wide applicability[25] because their properties are highly tunable changing physicochemical parameters.[26]

The *C. ciliaris* (African foxtail grass or buffelgrass) is a grass species, belongs to the Poaceae family, and is native to South Africa, north tropical and Asia.[27] It is also easily available in Pakistan and used in folk remedies for tumors, sores, kidney pain and wounds.[28] Related species of *C. ciliaris* are reported to be diuretic, emollient and anodyne.[28] Firstly, biosynthesis of Ag-NPs was carried out by using seed extract of *C. ciliaris*. The efficiency of silver ions (Ag^+) reduction, as well as the production of Ag-NPs from $AgNO_3$ solution with various compositions of *C. ciliaris* seeds exudate, was monitored using various characterization techniques.

The current work is devoted to investigate antibacterial activity of *C. ciliaris* Ag-NPs against gram-positive and negative strains and reduce the detrimental effects of toxic chemicals on the environment by decreasing the dye concentration (CR and MB) through employing *C. ciliaris*-capped Ag-NPs as a nano-catalyst. Moreover, adsorption of two models ACD (Dox and Dono) were used to study drug loading capacity and adsorption mechanism by kinetic modeling that might be helpful for the establishment of nano-scale drug delivery systems in future.

2. MATERIALS AND METHODS

2.1. Materials

Silver nitrate ($AgNO_3$), methylene blue (MB), congo red (CR) and sodium borohydride ($NaBH_4$) were procured from Sigma-Aldrich. All glass wares were cleaned with aqua regia and rinsed several times with double distilled water. Nutrient Agar was obtained from Bio Word. Pure cultures of the bacterial strains were received from Department of Zoology, G.C. University, Lahore. ACD loading as Daunorubicin (Dono) and doxorubicin hydrochloride (Dox) (Pharmedic Laboratories (Pvt.) Ltd., Lahore) were used for drug loading. Seeds (*C. ciliaris*) were collected from Jahangir Tomb Lahore, Pakistan. All materials were used as received.

2.2. Seed Exudate Preparation

The *C. ciliaris* seeds were collected from Lahore, Pakistan and washed thoroughly using deionized water thrice time prior to use. For the preparation of aqueous exudate, 10 g seed was suspended in 100 ml of deionized water for 24 h, filtered through a Whatman No.1-125mmO filter paper and used for present study.

2.3. Ag-NPs Synthesis

Biological synthesis of Ag-NPs was carried out by mixing various concentrations (10, 20, 30, 40 and 50 vol. %) of *C. ciliaris* seed exudate (labeled as 1CC, 2CC, 3CC, 4CC and 5CC) with (1 mM) aqueous $AgNO_3$ solution and incubated overnight at room temperature. Aqueous $AgNO_3$ (1 mM) acted as the silver salt precursor for the reduction of Ag^+ into Ag atoms.[29] The color of the solution turned from pale yellow to wine red and then light brown after 30 mints (constant stirring at 100 °C:pH 8) indicating the formation of silver nanoparticles.

2.4. Catalysis

Freshly prepared (0.5 mL) 0.1 M sodium borohydride solution was mixed with 3 mL aqueous methylene blue (0.03×10^{-3} M) and congo red (0.06×10^{-3} M) solution, respectively. Then 0.4 mL silver colloid of certain concentration was added to the solutions and agitated for five minutes. The decolourisation of the mixture represents the degradation of dyes. Methylene blue became colourless in the presence of reducing agent ($NaBH_4$) representing the reduction of methylene blue to leucomethylene blue (LMB).[30] The reaction in the absence of nanocatalyst is conducted as a reference. The absorption spectrum was evaluated at 2 min intervals in the range of 200–800 nm using UV-Vis spectrophotometer.

2.5. Drug Loading

2.5.1. Doxorubicin (Dox) Loading

Initially, individual drug solution of Dox and Dono was prepared by dissolved 5 mg drug in water 100 mL. These solutions were analyzed by UV-visible spectrophotometer between 400–600 nm as a control sample (0 minute). Then, 10 mg Ag-NPs was added in each solution with particle concentration 100 mg/L and placed in horizontal shaker at moderate frequency. Adsorption and concentration responses of drugs were noted by taking 2.5 mL of unbound drug supernatant at different time intervals (30, 60, 120, 240 and 480 min.) for measuring drug loading capacity evaluated by UV-visible absorption at 480 nm.

2.5.2. Loading Capacity

Loading capacity (LC) and Loading efficiency (LE) of Dox and Dono were calculated by subsequent Eq. (1) respectively.[31, 32]

$$\text{Loading capacity of drug } \left(\frac{\text{mg}}{\text{mg}}\right) = \frac{(\text{Drug}_i) - (\text{Drug}_f)}{(\text{Drug}_c)} \quad (1)$$

$$\text{Loading efficiency \% of drug} = \frac{(\text{Drug}_i) - (\text{Drug}_f)}{(\text{Drug}_i)} * 100 \quad (2)$$

Drug_i is the initial quantity (mg) of the drug, Drug_f is the free drug present in the supernatant and Drug_c is the quantity (mg) of carrier (Ag-NPs drug cargo).

2.6. Kinetics Data Analysis

In this work, four common kinetic methods (Lagergren pseudo first order, Pseudo-second order, Elovich equation and Intra-particle diffusion models) were used to determine Kinetics of adsorption mechanism, mass transport processes, chemical reaction, comparison of experimental results and diffusion rate.

2.6.1. Pseudo First Order

The Lagergren pseudo first order equation can be presented as[33, 34]

$$\mathrm{Log}(q_e - q_t) = \log q_e - \frac{k_1}{2.303}t \tag{3}$$

Where q_e and q_t are the drug/material absorbed by *C. ciliaris* Ag-NPs at equilibrium state and at certain time t respectively, k_1 is the constant of adsorption [1/min], by plotting graph of $\log(q_e - q_t)$ against t provides a linear relationship to compute the value of k_1 and q_e from the slope and intercept of graph line respectively.

2.6.2. Pseudo Second-Order Model

The linear form of pseudo-second order model is[35, 36]

$$\frac{t}{q_t} = \frac{1}{k_2 q_e^2} + \frac{t}{q_e} \tag{4}$$

The primary rate of absorption is

$$h = k_2 q_e^2 \tag{5}$$

$$\frac{t}{q_t} = \frac{1}{h} + \frac{t}{q_e} \tag{6}$$

Where k_2 shows the pseudo second order adsorption rate constant [g/mg min]. The values of k_2 and q_e can be computed from the intercept and slope of the graph of t/q_t against t.

2.6.3. Elovich Model

The Elovich model can be written as[37]

$$q_t = \frac{1}{\beta}\ln \alpha\beta + \frac{1}{\beta}\ln t \tag{7}$$

Here α represent initial adsorption rate [mg/g min] and β is called desorption constant [g/mg]. The plot between q_t and $\ln t$ gives a linear relationship and β and α are the intercept and slope of the plot.

2.6.4. Intra-Particle Diffusion Model

This model is widely used for adsorption studies here, k_i is the rate constants at stage i and can be calculated by following equation:[38]

$$q_t = k_i t^{1/2} + C_i \tag{8}$$

2.7. Antibacterial Activity

2.7.1. Bactericidal Potential of C. ciliaris Ag-NPs

Antibacterial activity of synthesized silver nanoparticles was investigated using locally isolated bacterial strains including (a) *Staphylococcus warneri* (KP117257), (b) *Staphylococcus aureus*, (c) *Bacillus anthracis* (KT356280), (d) *Acinetobacter baumannii* and (f) *Escherichia coli*. Bacterial strains were maintained in nutrient agar (composition gL^{-1}:peptone-5.0; meat extract-1.0; yeast extract-2.0; sodium chloride-5.0 and agar-20) slants. Well diffusion assay was used to evaluate the susceptibility of silver nanoparticles against chosen bacterial strains. The agar medium was sterilized in an autoclave at a pressure for 30 min. Following which the medium was transferred into sterile Petri dishes, after solidification bacterial suspensions containing 10^7 cells mL^{-1} were spread on the solid surface of media using a sterile cotton swab. Later with the help of sterilized borer, wells were punched in the agar plates to pour the different NPs. Different concentrations of biosynthesized Ag-NPs were used to determine the bactericidal potential. 50 μL (12 $\mu g \cdot mL^{-1}$) of each sample was applied to various strains. Samples were incubated overnight at 37 °C and zones of inhibitions were calculated with meter ruler.

2.7.2. Scanning Transmission Electron Microscopy (STEM)

Each bacterial sample was diluted into PBS and a 10 μL sample drop was deposited on TEM copper grids with a holey carbon film. The grid was then exposed to 70% glutaraldehyde vapours for 3 h to fix the samples. In order to estimate the distribution and location of the silver nanoparticles as well as morphology of bacteria after silver nanoparticles treatment, strains were analyzed in a JEOL 2100F TEM at an accelerating voltage of 200 KV in STEM mode. The presence of silver nanoparticles was verified by energy-dispersive X-ray spectroscopy (EDS) analysis.

2.8. Materials Characterization

UV-Vis spectrophotometer (TECAN infinite M200PRO) was used for absorption spectra of different Ag-NPs colloids. The structural and phase information of Ag-NPs were confirmed by X-ray diffraction (XRD) BRUKER D2 PHASER with the 2θ range of 10°–80°. The morphology and size of Ag-NPs were measured through transmission electron microscopy (TEM) through using Hitachi H7100FA TEM at 100 kV. EDX analysis is also conducted by using Hitachi H7100FA TEM scanning electron microscopy. TEM samples were prepared by dropping colloidal solution on holey carbon grids and evaporate them at room temperature. The functional group of NPs was analyzed using BRUKER ALPHA Platinum ATR spectrometer.

3. RESULTS AND DISCUSSION

Optical properties of Ag-NPs synthesized by different concentrations of the seed extract were tested using UV-Vis spectrophotometer. It can be observed that maximum

absorption was observed around 412 nm by 1CC (Fig. 1). The increasing concentration of seed extract is accompanied by a significant decrease in absorption intensity and broader surface plasmon resonance (SPR) peaks. Broader peaks of 3–5CC suggest the presence of nanoparticle's agglomeration. The reaction mixture alters the colour from light yellow to wine red and also light brown, by incorporating different compositions of *C. ciliaris* seed extract (Fig. 1(c)). *Setaria verticillata* seed extract recorded sharp peak of Ag-NPs at 40 vol.%[1] while in *C. ciliaris* 10–20 vol.% give sharp high intensity spectra demonstrating the best composition for NPs synthesis. The colour changes as a result of SPR vibration in the Ag-NPs. The dark brown colour of Ag-collide is recognized as SPR vibration due to free electrons induced by an electromagnetic field.[39,40]

The FTIR spectra of the Ag-NPs synthesized at the various *C. ciliaris* concentrations was obtained to identify the functional groups present (Fig. 1(b)). The FTIR signal

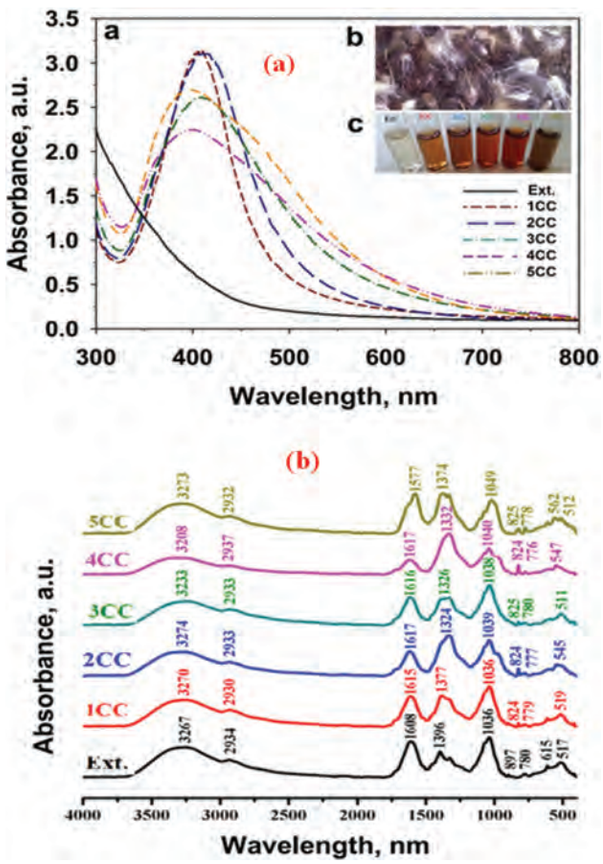

Fig. 1. (a) The UV-vis absorption spectra of synthesized Ag-NPs with extract. The wavelength of maximum absorption peak was around 412 for 1CC, ~406 for 2CC, 408 for 3CC, 396 for 4CC and 398 for 5CC, respectively. (b) *C. ciliaris* seeds (c) visual appearance of vials containing different concentrations of *C. ciliaris* seed extract, from 10–50 vol.%, mixed with 1 mM silver nitrate, from left to right. (b) FTIR spectrum of synthesized silver nanoparticles using *C. ciliaris* seed extract at various concentration.

of crude *C. ciliaris* seed extract was observed at 3276, 2934, 1608, 1396, 1036, 897, 780, 615 and 517 cm^{-1}. Absorption spectra at 3276 cm^{-1} correspond to alcoholic O–H stretching.[14] The band 2934 cm^{-1} is due to aldehydic C–H stretching and is shifted towards lower wavenumber (2930 cm^{-1}) which is attributed to the surface binding of Ag-NPs. The band at 1608 cm^{-1} can be assigned as amide 1 arise due to the carbonyl group and NH stretching vibrations in amide linkage of protein and shifting from 1608–1617 cm^{-1} was attributed to the binding of a carbonyl group with Ag-NPs. Presence of flavonoids and reducing sugars is confirmed from the peak at 1396 cm^{-1} that indicates –OH bending vibrations. The peak at 1036 cm^{-1} is ascribed to the C–O–C stretching[41] which might be attributed to the reduction of Ag^{+}, as it was shifted towards higher wavenumber of 1049 cm^{-1}. The small peaks at 897, 780, 615 and 517 cm^{-1} are attributed to the aromatic ring. According to the FTIR analysis, the active functional groups in *C. ciliaris* and *Setaria verticillata* seed extract could lead to the reduction of Ag^{+} ions to Ag-NPs.[41] The proteins in seed extract attached with Ag-NPs through either cysteine residues or free amine groups and involved in the stabilization of Ag-NPs by the surface-bound proteins.[42]

Figures 2(a)–(h) depicts typical TEM images of the NPs synthesized with different seed extract concentrations and their particle size distribution. The morphology and grain size of the particles could be tuned by adjusting seed extract concentration. Spherical NPs were obtained from 10 vol.% *Setaria verticillata* seed extracts although, 40 vol.% extract leads to the formation of hexagonal, triangular and quasi spherical NPs. Seed extracts are varied in their chemical composition so it is necessary to optimum the concentration for synthesizing best NPs. Capping agents in the extract control the shape of NPs like celluloses and hemi-celluloses. It can be seen that 10 vol.% of extract led to the formation of smaller NPs while high vol.% of *C. ciliaris* caused the agglomeration of polydisperse Ag-NPs (Figs. 2(b–d)). Due to this higher concentration of seed extract, large number of Ag+ was reduced simultaneously, resulting in the formation of more agglomerations. Ag-NPs with different shapes were observed using TEM analysis (Fig. 2), with an average particle size (d_{TEM}) of 12 nm for 1CC. It is worth mentioning that a particle size distribution of 9–12 nm were found for 3–5CC.

Figure 3 shows XRD diffraction pattern of biosynthesized Ag-NPs. Seed extract was used as control sample resulting in no characteristics XRD pattern. In contrast, the XRD spectrum of the samples exhibits four sharp diffraction peaks which are indexed as (111), (200), (220), (311) of face-centered cubic symmetry of Ag with corresponding 2θ values of 38°, 46°, 64.5° and 78°, respectively (JCPDS 07-0783).[1,43,44] The average crystal size of the NPs was measured according to the Scherrer equation

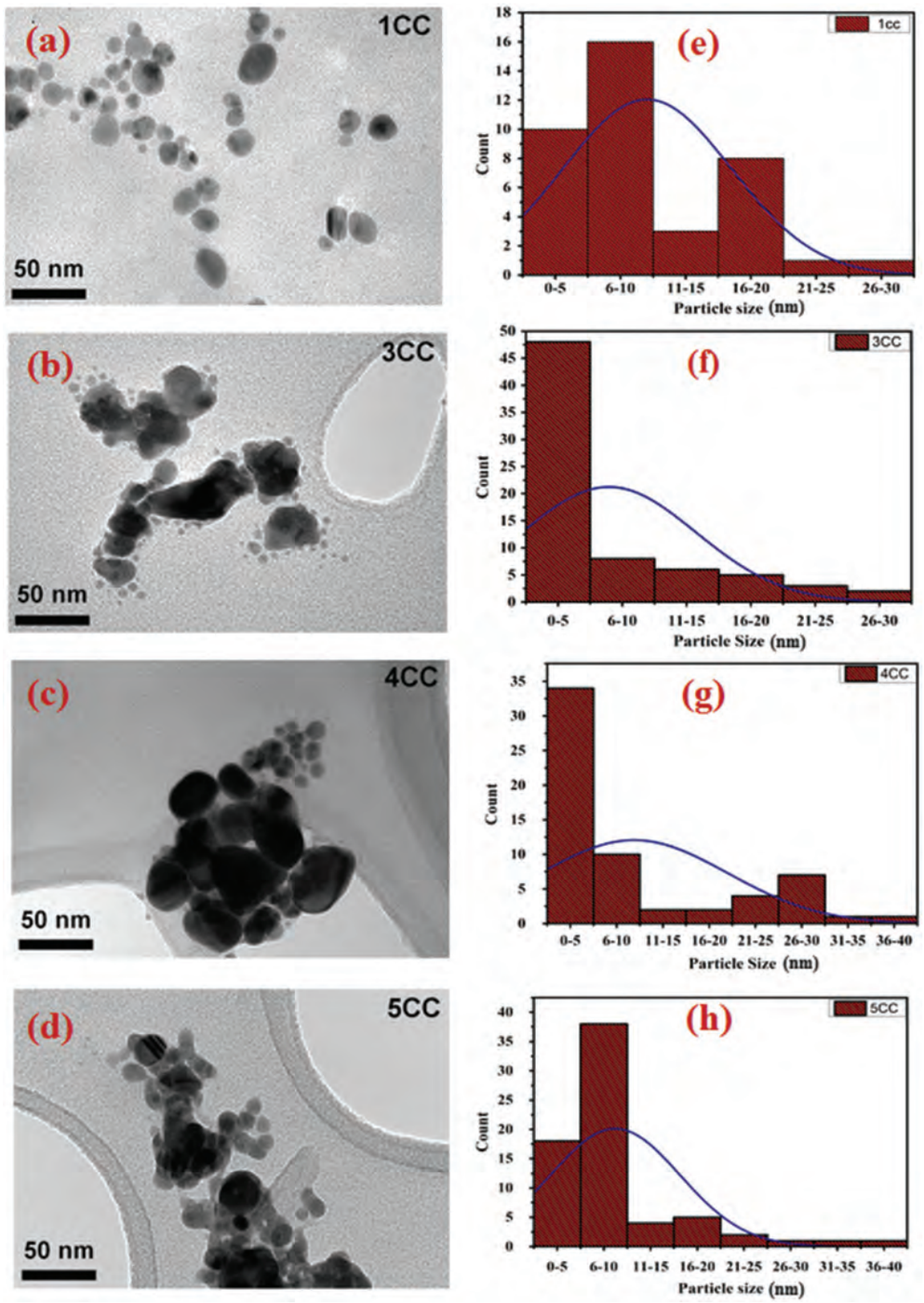

Fig. 2. TEM images of biosynthesized silver nanoparticles (a–d) and their particle size distribution (e–h) using *C. ciliaris* seed extract at different concentrations (a, e) 1CC; (b, f) 3CC; (c, g) 4CC and (d, h) 5CC incubated at 100 °C for 30 minutes at pH of 8.

(d_{XRD}) resulting in 13.5, 10.7, 11.8, 10.1 and 10.1 nm for 1 to 5CC NPs, respectively. The peak observed at 32° for 1CC might be attributed to bio-organic compounds present on the surface of NPs comes from seed extract. *Andean blackberry, Withania somnifera* and *Azadirachta indica* capped Ag-NPs also reported the peak at same position.[45–47] This might be attributed to bio-organic compounds present on the surface of NPs.[48, 49]

The catalytic reduction of MB and CR was investigated using $NaBH_4$ as the reducing agent and *C. ciliaris*-capped Ag-NPs as the nano-catalyst. Reducing capacity of $NaBH_4$ and seed extract with dye is not significant presented in

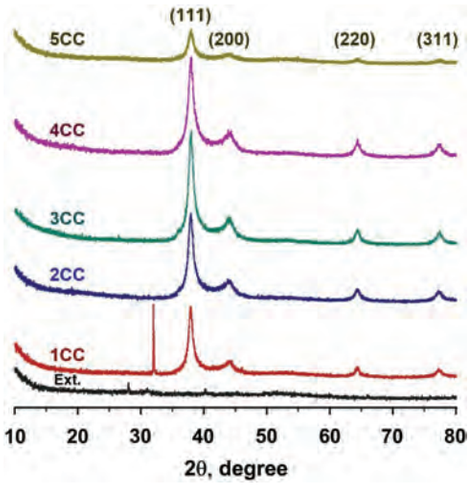

Fig. 3. XRD diffraction pattern of silver nanoparticles using *C. ciliaris* seed extract at various concentration.

Figures 4(a), (c) while the catalytic efficiency of *C. ciliaris* Ag-NPs (12 μg/ml) with $NaBH_4$ representing a quick successive decrease in concentration of dyes Figures 4(b), (d). Figure 4(b) depicts that relative absorption intensity was recorded at a regular interval of 2 min for a period of 16 min. The results display a complete reduction of MB to leuco methylene blue (LMB) at room temperature. *Biophytum sensitivum* capped Ag-NPs (0.020 mg/mL) degrade MB solution (0.08×10^{-3} M) in 9 min while *Azadirachta indica* capped Ag-NPs diminished MB (0.03×10^{-3} M) peak intensity in 13 min.[47,50] Similarly, the UV-Vis spectrum of the catalytic reduction of CR by $NaBH_4$ and *C. ciliaris* Ag-NPs (0.4 ml), degraded CR in 10 min presented in Figure 4(d). While *A. indica* (0.4 ml) and GT capped Ag-NPs reduce equimolar CR in 9–15 min representing significant efficiency of *C. ciliaris* nano catalyst.[47,51] In the aqueous reaction mixture of CR and $NaBH_4$ system, the maximum wavelength (λ_{max}) of 500 nm was achieved with a shoulder at 350 nm. The variations in the absorption intensity for both MB and CR depict a rapid reaction rate over a certain period of time. It can be observed that the rate of reaction increases with increasing the reaction time. In addition, the reduction of MB and CR was proximately completed at the end of the reaction period, demonstrating the influence of Ag-NPs. On the contrary, in the absence of the Ag-NPs, the reaction rate of reducing MB and CR was very slow, suggesting the catalytic function of Ag-NPs.

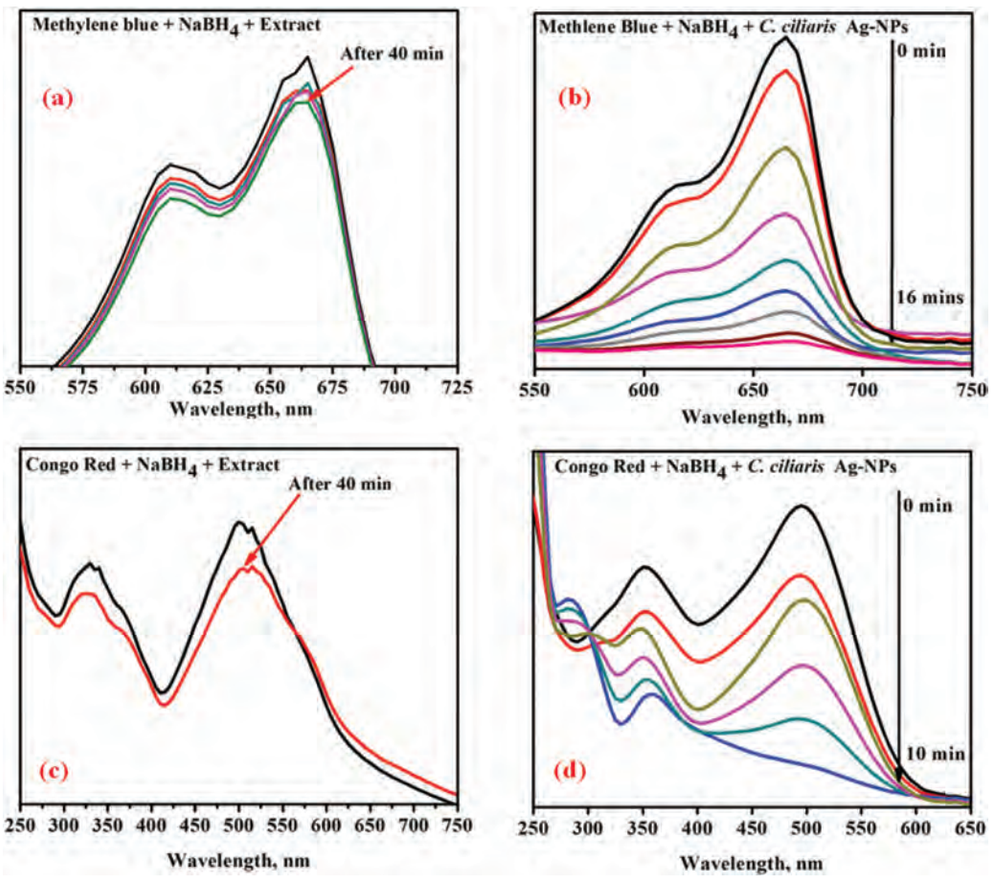

Fig. 4. UV-visible absorption spectrum for degradation of dyes, dye with $NaBH_4$ + *C. ciliaris* seed extract (a, c) and dye with $NaBH_4$ + *C. ciliaris* Ag-NPs (b, d).

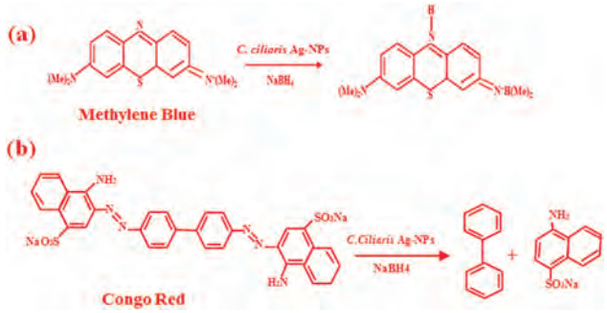

Fig. 5. Structure and reduced product of MB (a) and CR (b) by *C. ciliaris* Ag-NPs.

In the reaction mixture, a higher concentration of $NaBH_4$ was used as compared to MB and CR that increases pH of the whole system. This, in turn, results in retarding the degradation of BH_4-ions. The liberated H^+ ions create a purging atmosphere over the reaction mixture thereby effectively inhibiting the aerial oxidation of reduced MB and CR products. The catalytic degradation assisted by metallic nanoparticles is being effectively carried out by transferring electrons from electron donor species BH_4^- to electron acceptor species MB and CR mediated by *C. ciliaris*-capped Ag-NPs and thus reduces the activation energy and contributes to the stabilization of the system.[52] In the present report, the reduction reaction of *C. ciliaris* capped Ag-NPs displays good performance as a nano-catalyst and their catalytic product is presented in Figures 5(a), (b).

Figures 6(a)–(b) presents absorption spectra of hydrophilic ACD (Dox and Dono) supernatants collected at different time intervals (0–480 min.), the maximum peak intensity of ACD at zero time [$t = 0$] is controlled sample [free from *C. ciliaris* Ag-NPs]. Absorbance capacity of ACD increases as the time proceeds due to physisorption and chemisorption of the drug on the surface

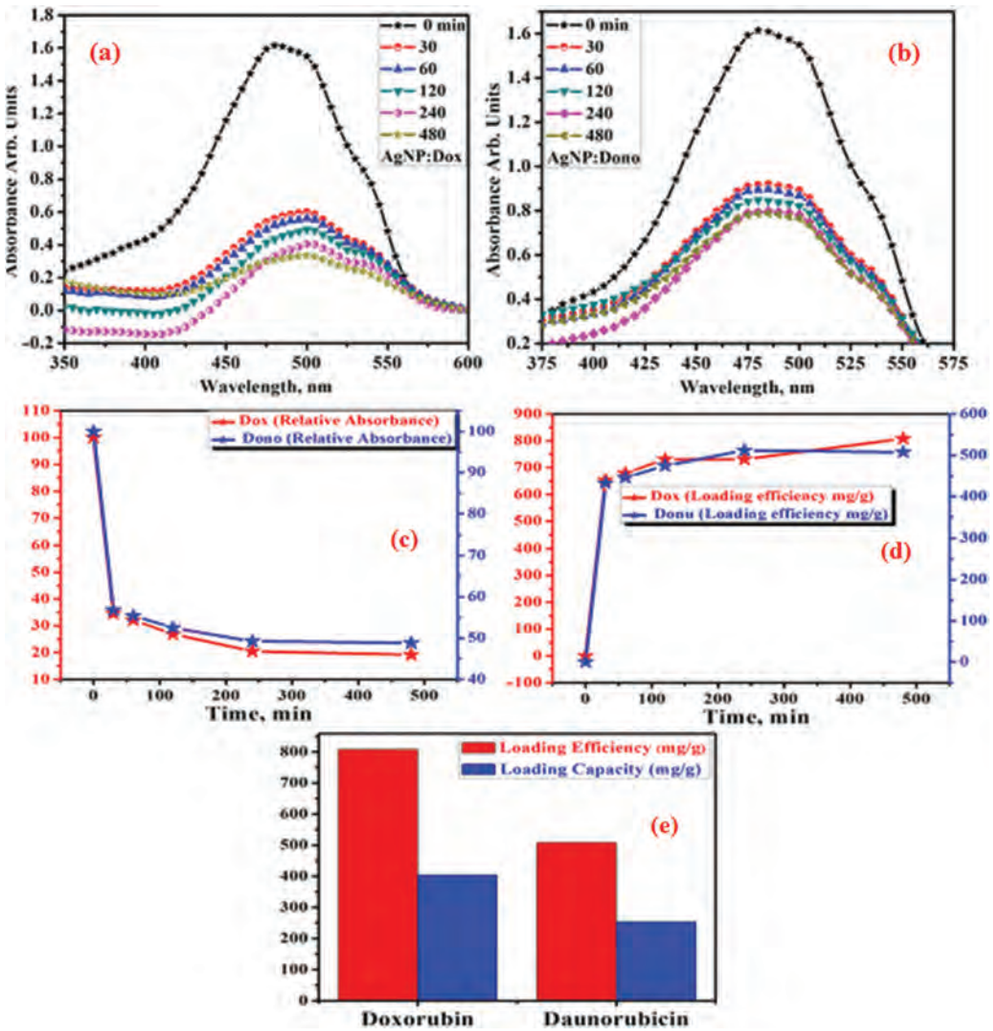

Fig. 6. Absorption spectra of (a) Dox and (b) Dono for various contact time ranges from 0–480 min. (c) Relative absorption (d) loading efficiency and (e) comparison of LC and LE for Dox and Dono.

of NP.[53] Physical adsorption is easily reversible as their binding energy is very low than chemisorption because of weak Vander wall forces while chemisorption is a kind of adsorption which involves a chemical reaction between the surface and the adsorbate and these bonds are stronger than physisorption. It can be seen that after 480 min, a minute quantity of adsorbed drug reclaimed by solution from weakly adsorbed on NPs by physisorption.[54] Figure 6 displays relevant absorption of drugs, an instant decrease in first 30 min attributes to large surface area, quick adsorption rate and high adsorption capacity of ACD on *C. ciliaris* Ag-NP.[55]

Figure 6(d) depicts efficiency of Dox and Dono after 480 minutes. Dox displayed relative low absorption (20%) as compared to Dono (48%). Although, Dox showed high loading efficiency and loading capacity 79% (795 mg/g) and 39.7% (397 mg/g) relative to Dono 50.7% (507 mg/g) and 25.35% (253.5 mg/g) respectively.[56] It is believed that relative low absorption capacity and high loading efficiency of Dox is because of comparatively strong hydrogen bonding, hydrophobic and ionic interactions between Dox and *C. ciliaris* Ag-NPs.

Adsorption mechanism of ACD was investigated by kinetic models and the efficacy of kinetic models was

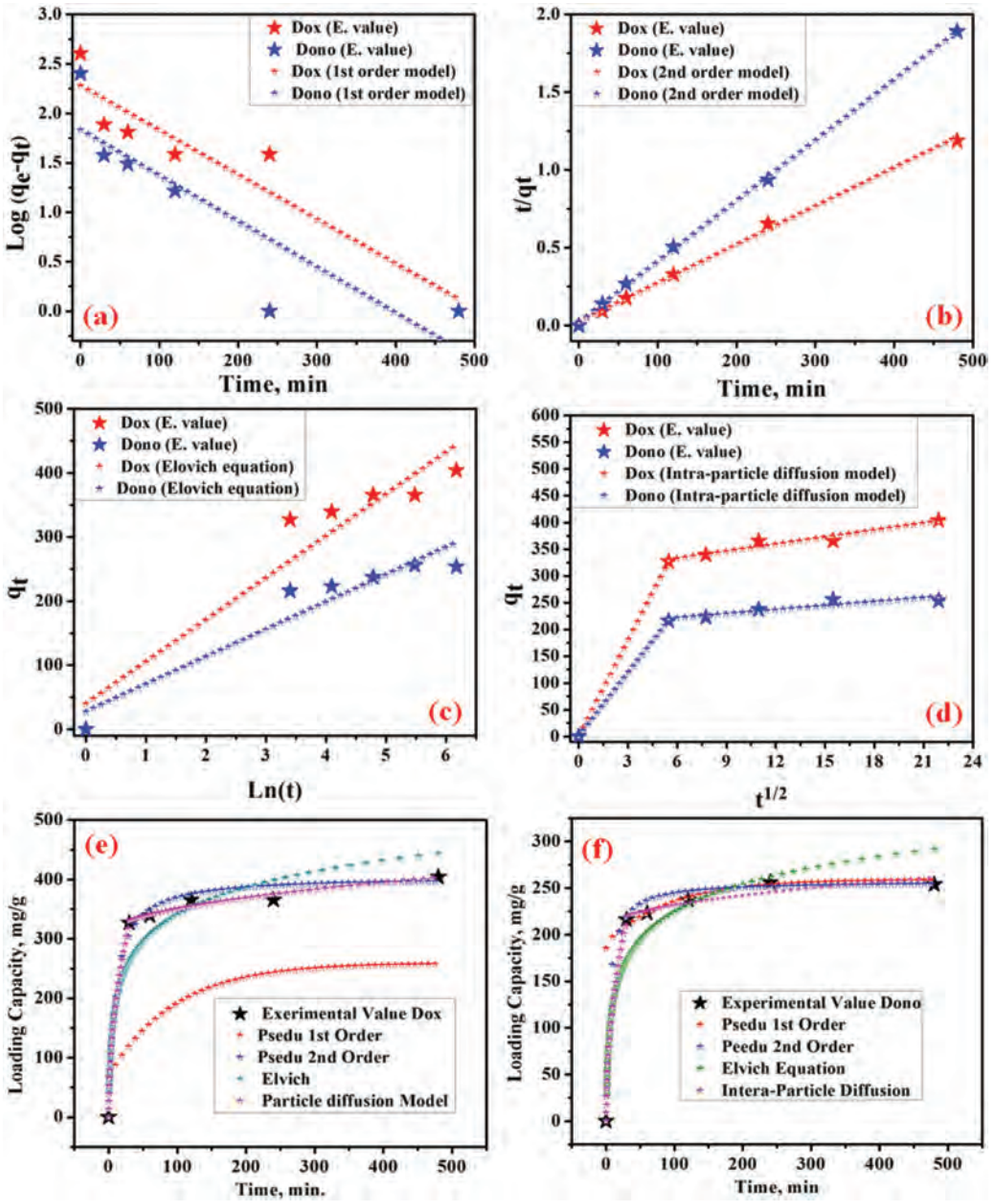

Fig. 7. Adsorption kinetics of Dox and Dono adsorbed by AgNPs: Pseudo-first-order (a), pseudo-second-order (b), elovich (c) and intra-particle diffusion models (d). Comparison between experimental adsorption capacities with calculated adsorption capacities of kinetics models: Dox (e) and Dono (f).

tested by the straight line fitting and is illustrated in Figures 7(a)–(f). The kinetics is typically explained by Lagergren pseudo first order and pseudo second-order models.[57] The corresponding kinetic parameters and coefficients of kinetic models are summarized in Table I. The values of the correlation coefficient obtained from the linear plot of pseudo-first order ($R_2 = 0.86485$, 0.71701) (Fig. 7(a)) and Elovich (Fig. 7(c)) models are much less ($R_2 = 0.89282$, 0.88268), demonstrating that the applicability of both kinetic models with reference to adsorption processes of ACD on *C. ciliaris* Ag-NPs is unfeasible. The experiments values (q_e, exp) were not in good agreement with theoretical values (q_e) for pseudo first order model. The higher correlation coefficient ($R_2 = 0.996$, 0.999) is attained for pseudo-second-order model (Fig. 7(b)), representing that, this model is good fit with experimental data and suggesting that adsorption processes of ACD on NPs involve chemical sorption and may have ion exchange phenomenon.[58]

In addition, results of Elovich model was not better fitted to experimental data (Fig. 7(c)) based on chemisorption with heterogeneous adsorbing surfaces, the adsorption rate decreases with time as an increase in surface exposure.[59, 60]

The intra-particle diffusion model can be employed to elaborate the adsorption mechanism. Figure 7(d) depicts that the plots of qt versus $t^{1/2}$ represent multi-linearity characterizations, showed that more than one diffusion step takes place. The first part is sharper and does not pass through the origin. It proposed that intra-particle diffusion is not only the rate controlling section but is also influenced by the boundary layer diffusion process.[34] The second subdued section is the low adsorption stage; where intra-particle diffusion starts to slow down, as minute concentration of ACD remain in solution.[61]

Figures 7(e)–(f) demonstrates that loading/adsorption capacity of ACD was calculated by different kinetic models and compared them with the experimental data. In the case of Dox, intraparticle diffusion model and pseudo-second-order model worked very well to explain the adsorption phenomenon. Elovich equation can also be employed to some extent to explain the adsorption behavior, but Pseudo-first-order model is totally failed to elaborate the adsorption process. The adsorption of Dono has the same behavior like Dox except for Pseudo-first-order model that is partially explaining the adsorption behavior can be seen in Figure 7(f).

Table I. Parameters of four kinds of kinetic models.

Kinetic model	Parameters	(Dox) values	(Dono) values
Pseudo first order	q_e (mg/g)	189.36	67.93
	K_1 (1/min)	−0.0103635	−0.01066289
	R^2	0.86485	0.71701
Pseudo second order	q_e (mg/g)	404.85	249.4
	h (mg/g min)	41.82	49.62
	K^2 (g/mg min)	2.55×10^{-5}	7.5×10^{-4}
	R^2	0.996	0.999
Elovich	α (mg/g min)	119	80.78
	β (g/mg)	0.01529	0.023394
	R^2	0.89282	0.88268
Intra-particle diffusion	k_I (mg/g·min$^{1/2}$)	59.72708	39.47122
	C_I (mg/g)	2.00972E–14	−2.00972E–14
	R^2	0.96975	0.94807
	k_{II} (mg/g·min$^{1/2}$)	4.38818	2.49138
	C_{II} (mg/g)	306.36038	206.621
	R^2	0.99858	0.98057

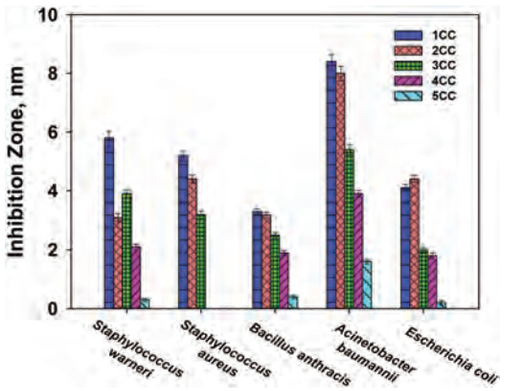

Fig. 8. Comparative analysis of antibacterial activity of *C. ciliaris* Ag-NPs in terms of zone of inhibition around the well. Ag-NPs prepared by using different concentration of *C. ciliaris* extract 10–50 vol.%, mixed with 1 mM silver nitrate. Each column represents the mean of three independent experiments.

Well diffusion assays were used to determine the antibacterial activity of *C. ciliaris* Ag-NPs. Antibacterial activity of 1CC and 2CC is greater than 3CC-5CC, in addition larger zone of inhibition was recorded for small size Ag-NPs (Fig. 8). These results agreed with previous work carried out by Rastogi and Arunachalam,[44] Jagtap and Bapat[63] and Mostafa M. H. Khalil (2014).[62–64] STEM images show that the Ag-NPs are distributed around bacterial strains *Staphylococcus aureus* and

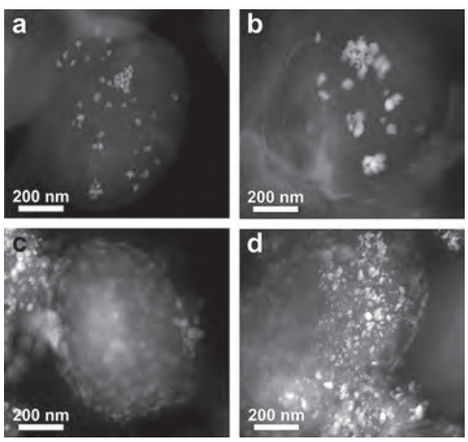

Fig. 9. (a–b) STEM images of nanoparticle treated *Staphylococcus aureus* (c–d) STEM images of nanoparticle treated *Acinetobacter baumannii* with elemental mapping. White spots indicate presence of silver.

Acinetobacter baumannii. According to the results presented in Figure 9, relatively more Ag-NPs are decorated on *Acinetobacter baumannii*. In fact, the different activities observed by Ag-NPs might be attributed to the cell wall composition.[65, 66] The strong interaction between Ag^+ and negatively charged bacterial walls probably facilitate the release of active Ag^+ into bacteria, resulting in an antimicrobial effect. The embedded Ag-NPs were located and represented as white colour dots in Figure 9.

4. CONCLUSIONS

This study summarizes the impact of *C. ciliaris* seed extract as a biological reducing agent for the synthesis of Ag-NPs, which can be easily scaled up due to its convenient, facile and eco-friendly features. Active functional groups present in FTIR spectra act as capping and reducing agents. The present investigation suggests that *C. ciliaris* capped NPs exhibited exceptional catalytic activity for the degradation of MB and CR in 16 and 10 min. respectively that offer an economic and efficient route to environmental protection. Ag-NPs adsorb the ACD and have proficient loading efficiency 80% and 50% respectively. The adsorption kinetic study shows that Ag-NPs had rapid adsorption rate and their kinetic data was in good agreement ($R^2 > 0.99$) with pseudo-second order and intraparticle model. Performance of elovich equation was also reasonable ($R^2 > 0.94$) for adsorption kinetic data. This work provides well concept of the adsorption mechanism between ACD and NPs to support bio-synthesized Ag-NPs based drug delivery systems. Bactericidal activity of 1CC and 2CC is greater as compare to other compositions because of small size factor. However, specific size nanoparticles fabrication using optimized reaction conditions might be an interesting area for future research.

Acknowledgment: Authors would like to thanks higher education commission (HEC) Pakistan through indigenous 5000 PhD fellowship program and gratefully acknowledges the support of Australian Research Council DP150101939, Australian Research Council DE160100569, and Westpac 2016 Research Fellowship. The authors wish to thank Dr. Noushin Nasiri (The School of Mathematical and Physical Sciences at UTS) regarding TEM images and Dr. Bushra Syeed (Department of Zoology, G.C.U. Lahore) for antimicrobial activity.

References and Notes

1. M. Naz, N. Nasiri, M. Ikram, M. Nafees, M. Qureshi, S. Ali, and A. Tricoli, *Appl. Nanosci.* 7, 793 (**2017**).
2. X. Xie, X. Shao, W. Ma, D. Zhao, S. Shi, Q. Li, and Y. Lin, *Nanoscale* 10, 5457 (**2018**).
3. Q. Zhang, S. Lin, S. Shi, T. Zhang, Q. Ma, T. Tian, T. Zhou, X. Cai, and Y. Lin, *ACS Appl. Mater. Interfaces* (**2018**).
4. S. Maiti, G. Barman, and J. K. Laha, *Appl. Nanosci.* 6, 529 (**2016**).
5. Q. Li, D. Zhao, X. Shao, S. Lin, X. Xie, M. Liu, W. Ma, S. Shi, and Y. Lin, *ACS Appl. Mater. Interfaces* 9, 36695 (**2017**).
6. K. Roy, H. Q. Mao, S. K. Huang, and K. W. Leong, *Nat. Med.* 5, 387 (**1999**).
7. E. Sachlos, D. Gotora, and J. T. Czernuszka, *Tissue Eng.* 12, 2479 (**2006**).
8. A. Vaseashta and D. Malinovska, *Sci. Technol. Adv. Mater.* 6, 312 (**2005**).
9. Q. Zhang, S. Lin, T. Zhang, T. Tian, Q. Ma, X. Xie, C. Xue, Y. Lin, B. Zhu, and X. Cai, *Cell Prolif.* 50 (**2017**).
10. T. Zhang, S. Lin, X. Shao, Q. Zhang, C. Xue, S. Zhang, Y. Lin, B. Zhu, and X. Cai, *Cell Prolif.* 50 (**2017**).
11. V. Vidhu and D. Philip, *Micron* 56, 54 (**2014**).
12. S. V. Kulkarni, C. Blackwell, A. Blackard, C. Stackhouse, and M. Alexander, US Government Printing Office (**1985**).
13. H. Kusic, N. Koprivanac, and L. Srsan, *J. Photochem. Photobiol.* 181, 195 (**2006**).
14. K.-T. Chung and C. E. Cerniglia, *Mutation Research/Reviews in Genetic Toxicology* 277, 201 (**1992**).
15. L. Fan, B. Jin, S. Zhang, C. Song, and Q. Li, *Nanoscale* 8, 12553 (**2016**).
16. Y. Lv, F. Wang, W. Qian, and G. Sun, *Oncology Letters* 9, 1545 (**2015**).
17. P. Xue, L. Sun, Q. Li, L. Zhang, J. Guo, Z. Xu, and Y. Kang, *Colloids Surf. B* 160, 11 (**2017**).
18. P. Parhi and S. K. Sahoo, *J. Colloid Interface Sci.* 451, 198 (**2015**).
19. R. Misra, S. Acharya, and S. K. Sahoo, *Drug Discov. Today* 15, 842 (**2010**).
20. N. Hondow, R. Brydson, P. Wang, M. D. Holton, M. R. Brown, P. Rees, H. D. Summers, and A. Brown, *J. Nanopart. Res.* 14, 977 (**2012**).
21. T. Indira and P. Lakshmi, *Int. J. Pharm. Sci. Nanotechnol.* 3, 1035 (**2010**).
22. S. Kayal and R. V. Ramanujan, *J. Nanosci. Nanotechnol.* 10, 5527 (**2010**).
23. S. V. Vinogradov, *Curr. Pharm. Des.* 12, 4703 (**2006**).
24. Q. Zhang, S. Deng, K. Sun, S. Lin, Y. Lin, B. Zhu, and X. Cai, *Cell Prolif.* 50 (**2017**).
25. H. Hosseinkhani and M. Hosseinkhani, *Curr Drug Saf.* 4, 79 (**2009**).
26. M. H. Mohamed and L. D. Wilson, *Nanomaterials* 2, 163 (**2012**).
27. L. R. Humphreys, A Guide to Better Pastures for the Tropics and Sub-Tropics (**1980**).
28. J. A. Duke and K. Wain, Medicinal plants of the world, Computer index with more than 85, 3 (**1981**).
29. G. Gnanajobitha, G. Annadurai, and C. Kannan, *Int. J. Pharma Sci. Res.* 3, 323 (**2012**) .
30. K. Leonard, B. Ahmmad, H. Okamura, and J. Kurawaki, *Colloids Surf. B* 82, 391 (**2011**).
31. M. Mashhadizadeh and M. Amoli-Diva, *J. Nanomedicine Nanotechnol.* 3 (**2012**).
32. B. Sabeti, M. I. Noordin, S. Mohd, R. Hashim, A. Dahlan, and H. Akbari Javar, *Biomed. Res. Int.* 2014 (**2014**).
33. Y. S. Ho and G. McKay, *Water Res.* 34, 735 (**2000**).
34. J. Lin and L. Wang, *Front Environ. Sci. En.* 3, 320 (**2009**).
35. Y. S. Ho and G. McKay, *Process Biochem.* 34, 451 (**1999**).
36. W. H. Hsieh, W. T. Chiu, Y. S. Lee, and Y. S. Ho, *Scientometrics* 60, 105 (**2004**).
37. S. Chien and W. Clayton, *Soil Sci. Soc. Am. J.* 44, 265 (**1980**).
38. W. Cheung, Y. Szeto, and G. McKay, *Bioresour. Technol.* 98, 2897 (**2007**).
39. P. Mulvaney, *Langmuir* 12, 788 (**1996**).
40. J. Y. Song and B. S. Kim, *Korean J. Chem. Eng.* 25, 808 (**2008**).
41. H. Kusic, N. Koprivanac, and L. Srsan, *J. Photochem. Photobiol.* 181, 195 (**2006**).
42. A. Gole, C. Dash, V. Ramakrishnan, S. Sainkar, A. Mandale, M. Rao, and M. Sastry, *Langmuir* 17, 1674 (**2001**).

43. J. H. Lee, S. Kang, J. Y. Lee, and J. H. Jung, *Soft Matter.* 8, 6557 (**2012**).
44. L. Rastogi and J. Arunachalam, *Mater. Chem. Phys.* 129, 558 (**2011**).
45. G. Marslin, R. K. Selvakesavan, G. Franklin, B. Sarmento, and A. Dias, *Int. J. Nanomedicine* 10, 5955 (**2015**).
46. B. Kumar, K. Smita, L. Cumbal, and A. Debut, *Saudi J. Biol. Sci.* 24, 45 (**2017**).
47. M. Naz, A. Haider, M. Ikram, M. Z. Qureshi, and S. Ali, *Nanosci. Nanotechnol. Lett.* 9, 1649 (**2017**).
48. M. Amutha, P. Lalitha, and M. J. Firdhouse, *Cogn. J. Nanotechnol.* 2014 (**2014**).
49. W. R. Rajesh, R. L. Jaya, S. K. Niranjan, D. M. Vijay, and B. K. Sahebrao, *Curr. Nanosci.* 5, 117 (**2009**).
50. S. Joseph and B. Mathew, *J. Mol. Liq.* 204, 184 (**2015**).
51. M. K. Indana, B. R. Gangapuram, R. Dadigala, R. Bandi, and V. Guttena, *Anal. Sci. Technol.* 7, 19 (**2016**).
52. M. K. Indana, B. R. Gangapuram, R. Dadigala, R. Bandi, and V. Guttena, *Anal.* 7, 19 (**2016**).
53. P. Selvam, S. Marek, C. R. Truman, D. McNair, and H. D. Smyth, *Aerosol. Sci. Technol.* 45, 81 (**2011**).
54. K. Autumn, Y. A. Liang, S. T. Hsieh, W. Zesch, W. P. Chan, T. W. Kenny, R. Fearing, and R. J. Full, *Nature* 405, 681 (**2000**).
55. C. Schafer, S. C. Mhadgut, N. Kugyela, M. Torok, and B. Torok, *Catal. Sci. Technol.* 5, 716 (**2015**).
56. J. Y. Teo, W. Chin, X. Ke, S. Gao, S. Liu, W. Cheng, J. L. Hedrick, and Y. Y. Yang, *Nanomed. Nanotech. Biol. Med.* 13, 431 (**2017**).
57. Z. Q. Zhang, M. C. Liao, H. Y. Zeng, S. Xu, X. J. Liu, J. Z. Du, P. H. Zhu, and Q. J. Huang, *Appl. Clay Sci.* 102, 246 (**2014**).
58. Y. S. Ho and A. E. Ofomaja, *J. Hazard Mater.* 2006, 129 (**2006**).
59. F. C. Wu, R. L. Tseng, and R. S. Juang, *Journal. Chem.* 150, 366 (**2009**).
60. S. Wu, X. Zhao, Y. Li, Q. Du, J. Sun, Y. Wang, X. Wang, Y. Xia, Z. Wang, and L. Xia, *Materials* 6, 2026 (**2013**).
61. Z. Cheng, X. Liu, M. Han, and W. Ma, *J. Hazard Mater.* 182, 408 (**2010**).
62. L. Rastogi and J. Arunachalam, *Mater. Chem. Phys.* 129, 558 (**2011**).
63. U. B. Jagtap and V. A. Bapat, *Ind. Crops Prod.* 46, 132 (**2013**).
64. M. H. Khalil, E. H. Ismail, K. Z. El-Baghdady, and D. Mohamed, *Arab J. Chem.* 7, 1131 (**2014**).
65. J. S. Kim, E. Kuk, K. N. Yu, J.H. Kim, S. J. Park, H. J. Lee, S. H. Kim, Y. K. Park, Y. H. Park, and C. Y. Hwang, *Nanomed. Nanotech. Biol. Med.* 3, 95 (**2007**).
66. J. Thiel, L. Pakstis, S. Buzby, M. Raffi, C. Ni, D. Pochan, and S. I. Shah, *Small* 3, 799 (**2007**).

Received: 14 February 2018. Accepted: 20 June 2018.